

## Some Thoughts on the Convective Urca Process

JOSIAH SCHWAB<sup>1</sup>

<sup>1</sup>*Department of Astronomy and Astrophysics, University of California, Santa Cruz, CA 95064, USA\**

### ABSTRACT

I have repeatedly grappled with the question of how the convective Urca process affects stellar evolution, in particular during the high-density convective carbon burning that can occur in near-Chandrasekhar-mass white dwarfs. This manuscript collects some fragmentary thoughts from various failed and abandoned attempts. This is not a complete work, does not provide a comprehensive overview of the literature, and has no definitive conclusions. It is posted in the hope that some part of it might prove useful to someone at some point in the future. I also take this opportunity to include another important result of more general interest (Appendix B).

*Keywords:* White dwarf stars (1799), Nuclear physics (2077), Stellar convective zones (301)

### 1. OVERVIEW

The explosion of a (near) Chandrasekhar-mass, carbon-oxygen white dwarf ( $M_{\text{Ch}}$  CO WD) has long been understood as a potential progenitor of Type Ia supernovae (see review by [Hillebrandt & Niemeyer 2000](#), and references therein). In this scenario, the WD slowly grows via accretion of mass from a non-degenerate companion star. When the mass of the WD has increased sufficiently, such that its central temperature and density reach the conditions for carbon ignition, a phase of convective central carbon burning begins. This phase, often known as “simmering”, eventually ends when the burning becomes dynamical, leading to the formation of a deflagration and subsequently the explosion (e.g., [Woosley et al. 2004](#)).

Stellar evolution calculations aim to simulate the progenitor systems over the long timescales of WD growth up to as close to the moment of explosion as their modeling assumptions reliably allow. One of the long-standing challenges in following models through the simmering phase is the uncertain effects of the convective Urca process. An Urca process is a cyclic series of electron-capture and beta-decay reactions, each of which emits a neutrino that then free-streams from the star ([Gamow & Schoenberg 1940, 1941](#)). The central convection zone

during carbon burning can span several orders of magnitude in density, such that for some isotopes, electron-capture reactions are favored at the center and beta-decay reactions near the outer edge. Convective mixing enables the transport of material between these regions, leading to the operation of the convective Urca process ([Paczynski 1972, 1973](#)). The precise effects of the convective Urca process are a matter of long debate. But at a schematic level, the presence of this additional energy loss mechanism requires additional carbon to be burned in order to reach explosion. The total amount of carbon burned influences the neutron excess of the material (e.g., [Chamulak et al. 2008](#)) and thus the nucleosynthesis during the explosion.

The most detailed observational probe of Type Ia nucleosynthesis comes from elemental and isotopic abundance measurements made in supernova remnants. Because the nucleosynthesis is sensitive to the mass and metallicity of the exploding WD, this provides an opportunity to test and constrain explosion models (e.g., [Badenes et al. 2008; Martínez-Rodríguez et al. 2017](#)).

Theoretical predictions for the detailed nucleosynthesis the Chandrasekhar-mass Type Ia channel are dependent on an accurate treatment of the convective Urca process. A self-consistent treatment of the convective Urca process suitable for incorporation in stellar evolution codes is sorely needed; this would unlock the potential of existing and future observations to constrain supernova progenitor systems.

Corresponding author: Josiah Schwab  
[jwschwab@ucsc.edu](mailto:jwschwab@ucsc.edu)

\* Humble Fellow

In this paper, we discuss the potential effects of the convective Urca process and the challenges of modeling it in stellar evolution codes.

## 2. SETUP

We use Modules for Experiments in Stellar Astrophysics (MESA; Paxton et al. 2011, 2013, 2015, 2018, 2019) to construct stellar models of CO WDs during the simmering phase. Most of the calculations shown in this paper were performed in early 2020 with MESA development versions functionally equivalent to release r12778. Attempting to model high-density convective carbon burning with MESA proved to be a challenging problem that revealed a variety of bugs, inconsistencies, and shortcomings. A reader wishing to further explore these types of models should use a forthcoming MESA release (so one made later than October 2021) and carefully and skeptically evaluate the assumptions and outputs. In Appendix A, we provide a detailed discussion of the key MESA equations.

### 2.1. Initial Model

We use a toy model of an accreting CO WD that reaches central carbon ignition and continues into convective carbon burning. We start with a homogeneous  $1 M_{\odot}$  CO WD consisting of 70%  $^{12}\text{C}$  and 30%  $^{16}\text{O}$  by mass. This object then accretes material of the same composition at a rate  $\dot{M} = 3 \times 10^{-7} M_{\odot} \text{yr}^{-1}$ . During this evolution, compressional heating and neutrino cooling largely erase its previous history (e.g., Paczyński 1971; Brooks et al. 2016), so the choice of initial mass and central temperature are not particularly important. In more detailed models, there remains some diversity in the properties at ignition due to variations in the initial mass and initial central temperature (Lesaffre et al. 2006; Chen et al. 2014).

### 2.2. Input physics

We use the simple N1 nuclear network from Förster et al. (2010), which is specifically tailored for this phase of high-density hydrostatic carbon burning. Our nuclear reaction rates are primarily the MESA default rates drawn from JINA REACLIB (Cyburt et al. 2010), modified by the screening prescription of Chugunov et al. (2007). This is not a state-of-the-art carbon ignition curve (see e.g., Gasques et al. 2005; Yakovlev et al. 2006), but serves our purposes. We also use the Suzuki et al. (2016) reaction rate tables for the Urca process weak reactions and the  $^{13}\text{N}(e^-, \nu_e)^{13}\text{C}$  reaction rate is the same as that used in Piersanti et al. (2017) (G. Martínez-Pinedo 2017, private communication).

The Urca process operates via a number of pairs (e.g., Tsuruta & Cameron 1970). The most prominent in

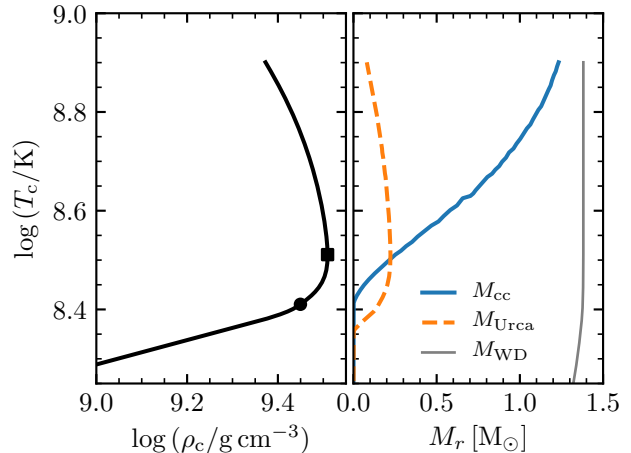


**Figure 1.** Evolution of our toy model. The left panel shows the evolution of the central temperature and density. Since the central temperature monotonically increases, it is a useful parameter for following the progress of the simmering. The right panel shows, at the time the model has that central temperature, the mass coordinate of the edge of the convective core and the mass coordinate of the Urca shell. The circle marks the point when the convective core forms; the square marks the point where the convective core first encompasses the Urca shell.

CO mixtures are  $^{21}\text{Ne}$ - $^{21}\text{F}$ ,  $^{23}\text{Na}$ - $^{23}\text{Ne}$ ,  $^{25}\text{Mg}$ - $^{25}\text{Na}$ , and  $^{25}\text{Na}$ - $^{25}\text{Ne}$  (Iben 1978). Throughout this work we will focus exclusively on  $^{23}\text{Na}$ - $^{23}\text{Ne}$ , as this pair is the most abundant initially and is also directly produced by carbon burning. Therefore, we when refer to any Urca-related concept (e.g., location of the Urca shell) throughout this paper, it is always with this pair in mind. The threshold density for this pair is  $\approx 1.9 \times 10^9 \text{g cm}^{-3}$ .

We use the HELM equation of state (Timmes & Swesty 2000), as implemented in MESA, throughout the star.<sup>1</sup> (This includes regions that would normally be covered by other EOSes.) Our motivation for this is that some of the experiments we undertake benefit from using the identical EOS through the star as EOS blends can be a source of spurious entropy generation.

## 3. A SIMPLE REFERENCE MODEL

We begin with a WD model that contains 70%  $^{12}\text{C}$  and 30%  $^{16}\text{O}$  by mass. It does not contain any Urca-pair isotopes. We then evolve this model in MESA with composition changes from nuclear reactions turned off

<sup>1</sup> When this work started, the Skye EOS (Jermyn et al. 2021) did not yet exist and the numerical properties of PC (Chabrier & Potekhin 1998; Potekhin & Chabrier 2000), as implemented in MESA, were not up to the task. Future work should certainly prefer Skye to HELM in these conditions.

(`dxdt_nuc_factor` = 0). This means that the WD remains chemically homogeneous throughout its evolution and thereby removes the necessity to model chemical mixing.<sup>2</sup> It also means that the outer convective boundary can be easily located via the Schwarzschild criterion.<sup>3</sup>

While this may seem an extreme assumption, only  $\approx 0.02 M_\odot$  of  $^{12}\text{C}$  are required to be burned to raise the WD to the temperature at which simmering ends (and the stopping condition of our calculations) of  $T_c = 8 \times 10^8 \text{ K}$  (Woosley et al. 2004). Therefore, the bulk composition does not dramatically change during simmering. This simplified model will provide a blank canvas on which to paint our thoughts.

Figure 1 summarizes the evolution of this model. The left panel shows the evolution of the central density and temperature. The WD is initially compressed by the accretion, but then as carbon burning proceeds and the convective core heats up, the WD hydrostatically adjusts and the central density falls. The right panel shows the extent of the central convective zone. The Urca shell (defined as the place where  $\lambda_{\text{ec}} = \lambda_\beta$ ) has a typical mass coordinate  $M_r \approx 0.2 M_\odot$  and is encompassed by the convective core.

### 3.1. Timescales

The long timescale in the problem is the mass growth timescale of the WD,

$$t_{\dot{M}} \equiv \frac{M}{\dot{M}} \sim 10^{14} \text{ s} \left( \frac{\dot{M}}{3 \times 10^{-7} M_\odot \text{ yr}^{-1}} \right)^{-1}, \quad (1)$$

assuming  $M \approx 1.4 M_\odot$ . Carbon burning effectively begins once its reaction timescale falls below this timescale and can run away once its energy generation rate exceeds rate of cooling via thermal neutrinos.

The short timescale is the dynamical timescale of the WD,

$$t_{\text{dyn}} \equiv \frac{1}{G\rho} \sim 0.1 \text{ s} \left( \frac{\rho}{10^9 \text{ g cm}^{-3}} \right)^{-1/2}. \quad (2)$$

As the timescale for carbon burning approaches the dynamical time, a deflagration will form.

There is a local heating timescale,  $t_{\text{heat,local}} = c_P T / \epsilon_{\text{nuc}}$ , but the convection zone is well coupled and

so local energy release is distributed across the whole convection zone. (The breakdown of this assumption is what ultimately ends simmering.) Therefore, following Piro & Bildsten (2008), we use the heating timescale associated with the the convection zone itself

$$t_{\text{heat}} = \left( \frac{d \ln T_c}{dt} \right)^{-1}. \quad (3)$$

Within the convection zone there is a minimum electron capture timescale,  $t_{\text{ec,min}}$ , and a minimum beta decay timescale,  $t_{\beta,\text{min}}$ . These are located at the center and at the outer edge of the convection zone, respectively. However, the reaction rates are significantly lower throughout most the convection zone, so an average timescale is also of interest. Define the mass-weighted average of a quantity  $x$  over the convective zone as,

$$\langle x \rangle \equiv \frac{1}{M_{\text{cc}}} \int_0^{M_{\text{cc}}} x \, dm. \quad (4)$$

Then these average timescales are  $t_{\text{ec}} = \langle \lambda_{\text{ec}} \rangle^{-1}$  and  $t_\beta = \langle \lambda_\beta \rangle^{-1}$ .

We can define an approximate advective mixing timescale across the convective core as

$$t_{\text{mix}} = \int_0^{r_{\text{cc}}} \frac{dr}{v_{\text{conv}}}, \quad (5)$$

where  $v_{\text{conv}}$  is the convective velocity reported by MESA via mixing length theory (MLT).

Figure 2 plots these timescales. The fact that the reaction timescales are often of order the mixing timescale is part of what makes modeling this process challenging. Except at the highest central temperatures, the reaction and mixing timescales remain well below the heating timescale. This means it can be reasonable to think about the interaction of reactions and mixing occurring at a fixed structure.

### 3.2. Neutrino luminosities

Given the sequence of WD structures from our toy reference model, we can calculate what the luminosity in Urca process neutrinos would be for assumed abundances and mixing properties.

Assume a total mass fraction of the Urca pair  $X_U$  that is constant throughout the convective region. We define the local fraction of the parent isotope as  $f_p$ . Then the luminosity is

$$L_U = \frac{X_U}{A_U m_u} \int_0^{M_{\text{cc}}} [f_p \epsilon_{\nu,\text{ec}} + (1 - f_p) \epsilon_{\nu,\beta}] \, dm, \quad (6)$$

where  $A_U = 23$ , the atomic mass number of our Urca pair of interest. To estimate  $f_p$ , we work in the same

<sup>2</sup> This circumvents the issues and shortcomings related to the interplay of reactions and mixing in MESA.

<sup>3</sup> The location of the outer convective boundary is influenced by the difference in composition between the contents of convection zone and the unmixed and unburned outer layers of the WD (Piro & Chang 2008).

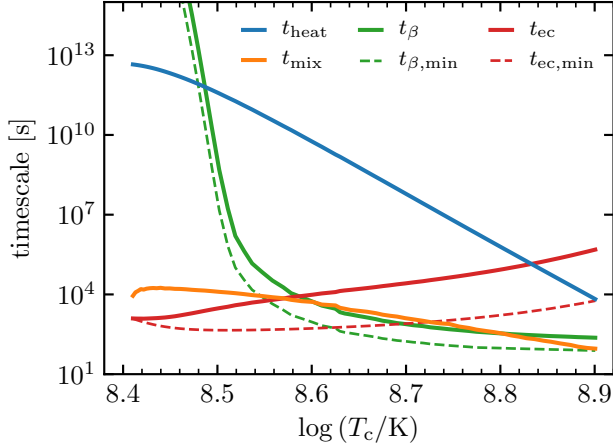


**Figure 2.** Timescales (as defined in the text) for our simple reference model.

diffusive mixing framework as is used in MESA. Assuming steady state abundances,

$$-f_p \lambda_{ec} + (1 - f_p) \lambda_\beta + \frac{\partial}{\partial m} \left( \sigma \frac{\partial f_p}{\partial m} \right) = 0 \quad (7)$$

where  $\sigma = D(4\pi r^2 \rho)^2$  is the Lagrangian diffusion coefficient. With the knowledge of  $D$ , we can then solve this equation to obtain the profiles within the convection zone.

### 3.2.1. No mixing ( $D = 0$ )

For  $D = 0$ , the problem is the same as for Urca cooling that occurs in stable radiative regions (i.e., thermal Urca process). This is effectively the minimum amount of cooling that can occur. The abundances are set by the local rate balance condition  $f_p \lambda_{ec} = (1 - f_p) \lambda_\beta$ . As a result,

$$L_{U,0} = \frac{X_U}{A_U m_u} \int_0^{M_{cc}} \left( \frac{\lambda_\beta \epsilon_{\nu,ec} + \lambda_{ec} \epsilon_{\nu,\beta}}{\lambda_{ec} + \lambda_\beta} \right) dm, \quad (8)$$

where  $\epsilon_{\nu,ec}$  and  $\epsilon_{\nu,\beta}$  are respectively the specific neutrino loss rates from electron capture and beta decay.

### 3.2.2. Instantaneous mixing ( $D = \infty$ )

We can also make the extreme assumption that the convection zone is instantaneously mixed. This will maximize the rate at which the convective Urca process can operate. Within the mixed region, uniform abundances of the parent/daughter Urca isotopes are set by the balance of the mass-weighted rates through the convection zone. Then the total Urca-process neutrino luminosity from the convective zone is

$$L_{U,\infty} = \frac{X_U M_{cc}}{A_U m_u} \left( \frac{\langle \lambda_\beta \rangle \langle \epsilon_{\nu,ec} \rangle + \langle \lambda_{ec} \rangle \langle \epsilon_{\nu,\beta} \rangle}{\langle \lambda_{ec} \rangle + \langle \lambda_\beta \rangle} \right). \quad (9)$$

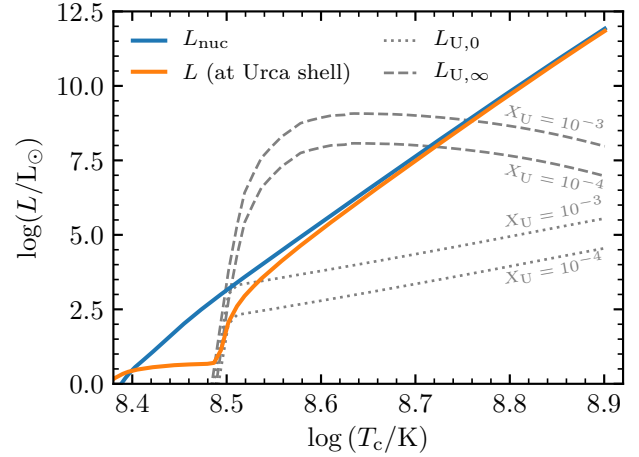


**Figure 3.** Characteristic luminosities as a function of central temperature. Solid lines show the total nuclear luminosity of the MESA models and the local luminosity at the Urca shell. Dashed lines are estimates of the minimum Urca-process neutrino luminosities (Equation 8). Dotted lines are estimates of the maximum Urca-process neutrino luminosities (Equation 9).

### 3.2.3. Results

Figure 3 puts the luminosity bounds from our estimates in Equations (8) and (9) in context. As a function of model central temperature, these are compared to the total nuclear luminosity. The convection zone encompasses the Urca shell around  $\log(T_c/K) \approx 8.5$ . From then, until  $\log(T_c/K) \gtrsim 8.75$ , the nuclear luminosity from carbon burning is well below the maximum neutrino luminosity, meaning the Urca process has the opportunity for maximum impact. Above that temperature, the carbon burning is sufficiently rapid that it cannot significantly influence the global energetics.

In Figure 4, we show the result of numerically solving Equation (7), assuming the structure from the MESA model at a particular time, for a range of constant  $D$ . This confirms the limiting behaviors derived analytically. It also indicates that the value of  $D$  reported by MESA MLT puts us in the limit of  $L_U \approx L_{U,\infty} \gg L_{nuc}$ .

### 3.3. Extent of convective core

If we assume that there is a central region that is being mixed infinitely fast, then the neutrino luminosity also depends on where the outer edge of this mixed region is placed. The estimate of Equation (9) assumes this mixed region corresponds to the convective region reported in the MESA models ( $M_{cc}$ ).

To illustrate the potential effect of the Urca process, we evaluate the neutrino luminosity assuming a centrally mixed region of size  $M_{mix} \leq M_{cc}$ . We define a critical

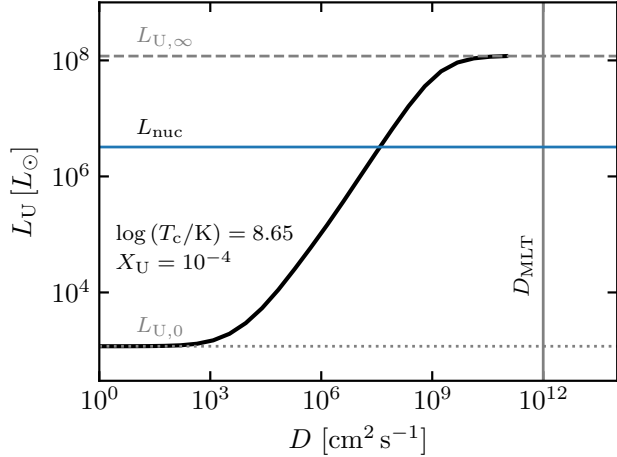


**Figure 4.** Neutrino luminosities from evaluating Equation (6) for the steady-state abundance profiles associated with a range of constant diffusion coefficients. This assumes the stellar structure of the MESA model at the indicated point in the evolution.

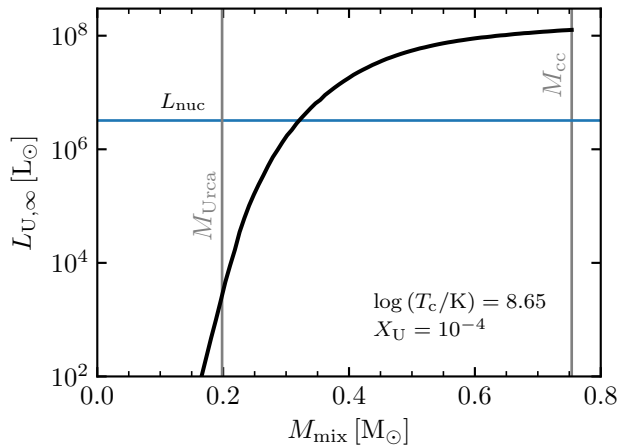


**Figure 5.** Illustration of finding  $M_{\text{mix,U}}$ , the point when  $L_{U,\infty} = L_{\text{nuc}}$ . This will be intermediate between the location of the Urca shell ( $M_{\text{Urca}}$ ) and the unmodified location of the convective core ( $M_{\text{cc}}$ ).

extent  $M_{\text{mix,U}}$  that occurs when  $L_{U,\infty} = L_{\text{nuc}}$ . Figure 5 visually illustrates this process for a single model snapshot. This calculation is not self-consistent as the temperature-density structure of the star is held fixed independent of size the hypothetically mixed region. Figure 6 shows the energy generation rate and cumulative luminosity associated with the Urca process superimposed on the background model. This illustrates that in a steady state, the neutrino cooling happens near the edges of the convection zone. In fact, the Urca shell is the location of the minimum neutrino cooling rate.

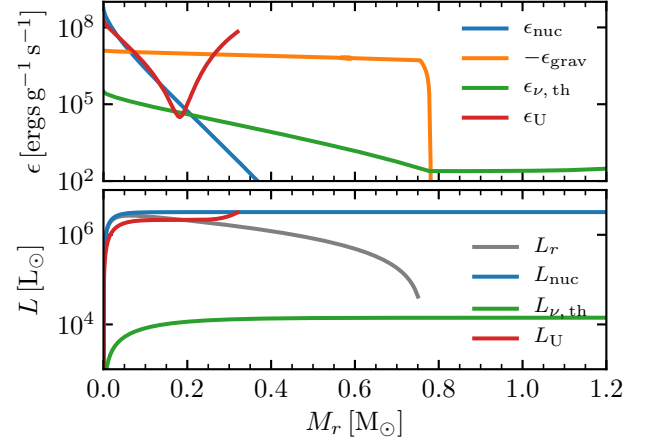


**Figure 6.** Local energy generation rates (top panel) and integrated luminosities (bottom) panel for the model shown in Figure 5.

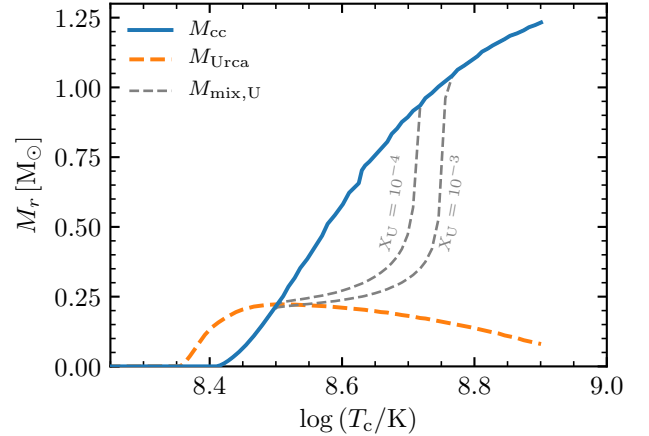


**Figure 7.** Size of the mixed region necessary to balance nuclear luminosity. Grey dashed lines show this extent for the two indicated values of the Urca isotope mass fraction. Balance is only possible when the grey curves are visible.

By repeating the procedure described above on the sequence of stellar structures from the simplified model, we map out how the size of this mixed region changes with central temperature. Figure 7 shows that the mixed region must generally extend somewhat beyond the Urca shell, but that the region may be significantly restricted.

This likely remains an overestimate of the size of the core. The luminosity profile throughout the convective region is affected by the fact that it is not in thermal equilibrium as work to expand the star is being performed on the heating timescale (Piro & Chang 2008). If the Urca cooling were to more nearly balance the nuclear heating, then the net heating (and expansion) timescale

would lengthen and expansion work would be done less rapidly. In the extreme limit where the heating and cooling balanced, the evolution would instead proceed on the timescale of the composition change.

#### 4. ONSET OF CONVECTIVE CARBON BURNING

When central carbon burning begins, the star is relatively quickly destabilized. The region where the carbon fusion is occurring is almost always above the  $^{23}\text{Na}$  threshold density, so that the  $^{23}\text{Na}(e^-, \nu_e)^{23}\text{Ne}$  reaction almost always occurs. This provides more nuclear energy per carbon burnt and also means that the Urca-pair composition of the convection zone will be primarily the  $^{23}\text{Ne}$ . Eventually, the convection zone grows to the location of the Urca shell. At that time there will be a  $^{23}\text{Ne}$  abundance that is the sum of the initial  $^{23}\text{Na}$  abundance and the  $^{23}\text{Na}$  produced thus far from carbon burning. This means there is a threshold metallicity below which the Urca-pair abundance in the convection zone at the time of formation of the Urca shell is approximately constant.

#### 5. THE CONVECTION ZONE REACHES THE URCA SHELL

There is a maximum luminosity that can be carried (radiatively) by stably stratified material, corresponding to the point where  $N^2 = 0$ . Typically, this corresponds to the adiabatic stratification ( $\nabla_T = \nabla_{\text{ad}}$ ). However, there can be an additional enhancement in the presence of stabilizing composition gradients. That is, we have  $\nabla_{\text{ad}} < \nabla_T \leq \nabla_{\text{ad}} + B$ , and so a luminosity

$$L_{\text{max}} = \frac{16\pi acGM_r T^4}{3\kappa P} (\nabla_{\text{ad}} + B). \quad (10)$$

When the composition dependence of the pressure is through the electron fraction, as in degenerate material, the Brunt term for stability can be written as

$$B = -\frac{1}{\chi_T} \left( \frac{\partial \ln P}{\partial \ln Y_e} \right)_{\rho, T} \frac{d \ln Y_e}{d \ln P}. \quad (11)$$

We can make a simple estimate for the value of  $B$  in these circumstances. For a cold plasma with degenerate electrons and ideal ions,  $(\partial \ln P / \partial \ln Y_e)_{\rho, T} \approx 4/3$  and  $\chi_T \approx 4kT / (\bar{Z} E_F)$ . Given a mass fraction  $X_U \ll 1$  of an Urca isotope with mass number  $A_U$ , the change in electron fraction associated with the reaction is  $\Delta Y_e = -X_U / A_U$ . We can rewrite

$$\frac{d \ln Y_e}{d \ln P} = \frac{1}{Y_e} \frac{d Y_e}{d r} \frac{d r}{d \ln P} \approx \frac{1}{Y_e} \frac{\Delta Y_e}{\Delta r} H_P, \quad (12)$$

where  $\Delta r$  reflects the size of the Urca shell. The equilibrium shifts when the chemical potential changes by

$\approx kT$ , so  $\Delta r \approx 4(kT/E_F)H_P$ . For the typical conditions associated with  $^{23}\text{Na}$  and carbon simmering, this implies

$$B_{\text{max}} \approx X_U \left( \frac{\bar{Z}/A_U}{Y_e} \right) \left( \frac{4kT}{E_F} \right)^{-2} \quad (13)$$

$$\sim 0.6 \left( \frac{X_U}{10^{-4}} \right) \left( \frac{T}{2 \times 10^8 \text{ K}} \right)^{-2}. \quad (14)$$

This suggests that the composition gradient can provide some additional stabilization but not so much that convection would be unable to penetrate at the radius around the threshold density and set up the Urca shell.

#### 6. SUMMARY AND CONCLUSIONS

By using toy models and sacrificing some aspects of self-consistency, I made estimates about neutrino luminosities and convective core sizes that are relevant to the operation of the convective Urca process (Section 3).

My initial goal was to produce MESA models of white dwarfs undergoing high-density convective carbon burning and exhibiting local energy conservation. That seems a key milestone before one can hope to characterize the effect of a convective region containing an Urca shell in stellar models. (Subsequently, one can start to tackle questions of whether what is happening in the 1D stellar models is an accurate reflection of what happens in a real star.) Despite significant effort, I failed to realize that goal, but the attempts resulted in a number of improvements to MESA. I'm still not sure if it is possible, but it is less impossible than when I started.

I thank Carles Badenes, Lars Bildsten, Adam Jermyn, Samuel Jones, Stephen Justham, Daniel Lecoanet, Gabriel Martínez-Pinedo, Héctor Martínez-Rodríguez, Anthony Piro, Philipp Podsiadlowski, Eliot Quataert, Donald Willcox, Stan Woosley, and Michael Zingale for helpful conversations on this and related topics.

Josiah was supported by NASA through Hubble Fellowship grant HST-HF2-51382.001-A awarded by the Space Telescope Science Institute, which is operated by the Association of Universities for Research in Astronomy, Inc., for NASA, under contract NAS5-26555, by the A.F. Morrison Fellowship in Lick Observatory, by the NSF through grant ACI-1663688, via support for program number HST-GO-15864.005-A provided through a grant from the STScI under NASA contract NAS5-26555, and by his wife Annelise Beck. Josiah's computer was supported by Bill Paxton's Stanford yearbooks and an Interlisp reference manual.

## APPENDIX

## A. CONSERVATION LAWS AND THERMODYNAMICS

Understanding the way that energy conservation is encoded in the stellar structure equations can prove confusing, especially in the presence of composition changes due to nuclear reactions and chemical transport processes. Here we carefully work through how conservation principles and thermodynamics lead to the stellar structure equations. We then discuss various limitations and approximations that are (or have been) present in the MESA implementation of these equations.

A.1. *Baryon Number*

Since nuclear reactions involve changes in mass, it is important that we work in the conserved physical quantity, which is the baryon number  $N_B$ . Denoting Avogadro's number by  $N_A$ , the atomic mass unit is  $m_u = 1 \text{ g}/N_A$ . The number abundance of every species is defined with reference to the baryonic number density,  $Y_i \equiv n_i/n_B$ . The total baryonic mass density is  $\rho = n_B/N_A$ , so that  $1/\rho$  is the specific volume. Local charge neutrality and local thermodynamic equilibrium (LTE) determine a unique solution for the ionization state of each isotope. Thus, the composition is completely specified by a set of number abundances  $\{Y_i\}$  for all nuclear isotopes and electrons are not a separately tracked species. The mass fractions are  $X_i = A_i Y_i$ , where  $A_i$  is the nucleon number; by construction  $\sum_i X_i = 1$ .

The specific rest mass energy density is

$$e_{\text{rest}} = \sum_i N_A M_i c^2 Y_i \quad (\text{A1})$$

Our definition of rest mass is the atomic mass (or atomic mass excess). The atomic mass includes the rest mass of the nucleus and electrons; it also includes the electron binding energy, which should not be present when material is fully ionized, but is typically negligible.

A.2. *Species and Mass Conservation*

The baryonic mass density of an individual species ( $\rho_i = \rho X_i$ ) is not conserved, but rather obeys the advection-diffusion equation,

$$\frac{\partial(\rho X_i)}{\partial t} + \nabla \cdot (\rho X_i \mathbf{v}) = \nabla \cdot (D \rho \nabla X_i) + \rho \dot{X}_i, \quad (\text{A2})$$

where  $D$  is a (species-independent) diffusion coefficient and  $\dot{X}_i = A_i \dot{Y}_i$  represents the rate of change of species  $i$  due to nuclear reactions. Summing the individual equations yields conservation of baryonic mass

$$\frac{\partial \rho}{\partial t} + \nabla \cdot (\rho \mathbf{v}) = 0. \quad (\text{A3})$$

since  $\sum_i \nabla \cdot (D \rho \nabla X_i) = \nabla \cdot (D \rho \nabla \sum_i X_i) = 0$  and we assume the reactions conserve baryon number.

Defining the usual Lagrangian derivative,

$$\frac{D}{Dt} = \frac{\partial}{\partial t} + \mathbf{v} \cdot \nabla, \quad (\text{A4})$$

and with the help of Equation (A3), we can rewrite Equation (A2) as

$$\rho \frac{DX_i}{Dt} = \nabla \cdot (D \rho \nabla X_i) + \rho \dot{X}_i. \quad (\text{A5})$$

Specializing to spherical coordinates, recall

$$\frac{\partial}{\partial r} = 4\pi r^2 \rho \frac{\partial}{\partial m} \quad (\text{A6})$$

and thus we can write

$$\frac{DX_i}{Dt} = \frac{\partial}{\partial m} \left( D (4\pi r^2 \rho)^2 \frac{\partial X_i}{\partial m} \right) + \dot{X}_i. \quad (\text{A7})$$

After defining the Lagrangian diffusion coefficient  $\sigma = D(4\pi r^2 \rho)^2$ , we arrive at the time evolution equations that MESA solves for the mass fractions  $X_i$  (see Equations 13-14 in Paper I),

$$\frac{DX_i}{Dt} = \underbrace{\dot{X}_i}_{\text{burn}} + \underbrace{\frac{\partial}{\partial m} \left( \sigma \frac{\partial X_i}{\partial m} \right)}_{\text{mix}}. \quad (\text{A8})$$

Traditionally we name the first term the “burn” part (the bulk term due to nuclear reactions, where  $\dot{X}_i$  comes from the `net` module) and the second term the “mix” part (the boundary term due to convective mixing, where  $\sigma$  comes from MLT).

### A.3. Thermodynamics

The first law of thermodynamics is a statement about energy conservation. In Paper IV, we derived a total energy equation by combining the first law with the momentum equation. Chapter II of [de Groot & Mazur \(1969\)](#) demonstrates that the first law comes from combining the more fundamental hydrodynamical equations that encode the conservation of mass, momentum, and total energy (see also Appendix A in [Bauer et al. 2020](#)). Assuming that there is not element diffusion (i.e., all species move with the same bulk velocity), their Equation (II.39) reduces to the familiar form

$$\frac{De}{Dt} = \frac{Dq}{Dt} - P \frac{D}{Dt} \left( \frac{1}{\rho} \right), \quad (\text{A9})$$

where  $e$  is the internal energy.

The “heat flow” term in Equation (A9) is

$$\frac{Dq}{Dt} \equiv \dot{q} - \frac{1}{\rho} \nabla \cdot \mathbf{J}_q. \quad (\text{A10})$$

This represents the total rate of the flow of energy into a Lagrangian parcel. The quantity  $\dot{q}$  is the specific volumetric source term, reflecting the rate of processes that can directly remove energy from the system (i.e., optically-thin cooling). The quantity  $\mathbf{J}_q$  is the heat flow and so this term reflects energy moving through the boundaries of a volume into adjacent regions.

### A.4. Local Energy Equation

In Paper IV, we stated that in the stellar structure equations, energy conservation is typically formulated by considering the energy flow in and out of a fluid parcel. This idea is an expression of the physics encoded by Equation (A10). Traditionally, we denote the specific volumetric source term as  $\epsilon$ .

As discussed previously, the conserved quantity is baryon number, so we define our Lagrangian coordinate to be the enclosed baryonic mass, i.e., the number of enclosed baryons times the atomic mass unit. This means that there can be a flow of rest mass energy through the boundary of a parcel. Then the total energy flow is

$$\mathbf{J}_q = \mathcal{F} - \sum_i D \nabla \left( M_i c^2 N_A \frac{\rho X_i}{A_i} \right), \quad (\text{A11})$$

where we represent the familiar flux of energy carried by radiation, convection, and conduction with  $\mathcal{F}$ . Recall that by the definition of  $L$ , under spherical symmetry

$$\frac{\partial L}{\partial m} = \frac{1}{\rho} \nabla \cdot \mathcal{F}. \quad (\text{A12})$$

Thus taking the divergence and inserting into Equation (A10), we see that the parcel obeys

$$\frac{Dq}{Dt} = \epsilon - \frac{\partial L}{\partial m} + \sum_i N_A \frac{M_i c^2}{A_i} \frac{\partial}{\partial m} \left( \sigma \frac{\partial X_i}{\partial m} \right). \quad (\text{A13})$$

The familiar form (Equation 54 in Paper IV) would be restored if we neglected the rest mass.



### A.5. Nuclear Reactions

Combining Equations (A9) and (A13) gives

$$\frac{De}{Dt} - \frac{P}{\rho^2} \frac{D\rho}{Dt} = \epsilon - \frac{\partial L}{\partial m} + \sum_i N_A \frac{M_i c^2}{A_i} \frac{\partial}{\partial m} \left( \sigma \frac{\partial X_i}{\partial m} \right). \quad (\text{A14})$$

We separate out the rest mass energy density,

$$\frac{De}{Dt} = \frac{De_{\text{rest}}}{Dt} + \frac{De_{\text{int}}}{Dt} = \sum_i N_A M_i c^2 \frac{DY_i}{Dt} + \frac{De_{\text{int}}}{Dt} \quad (\text{A15})$$

Taking Equation (A8) and dividing by  $A_i$  gives an equation for  $DY_i/Dt$ . Inserting this gives

$$\frac{De}{Dt} + \sum_i N_A M_i c^2 \dot{Y}_i - \frac{P}{\rho^2} \frac{D\rho}{Dt} = \epsilon - \frac{\partial L}{\partial m}. \quad (\text{A16})$$

where the rest mass flow term has been canceled by the mixing-related part of the  $De/Dt$  term. A typical definition of  $\epsilon_{\text{nuc}}$  (e.g., Equation 11 in Hix & Meyer 2006) is

$$\epsilon_{\text{nuc}} = - \sum_i N_A M_i c^2 \dot{Y}_i, \quad (\text{A17})$$

and we immediately see that term is present in Equation (A16). If rest mass is included in the definition of energy, then  $\epsilon_{\text{nuc}}$  is not separately inserted into  $\epsilon$  in Equation (A13). The value of  $\epsilon$  is only optically-thin cooling, which consists of both thermal ( $\epsilon_{\nu,\text{th}}$ ) and nuclear ( $\epsilon_{\nu,\text{nuc}}$ ) neutrinos. The specific nuclear neutrino loss rate is

$$\epsilon_{\nu,\text{nuc}} = \sum_i \langle E_\nu \rangle \dot{Y}_i. \quad (\text{A18})$$

So we now have

$$\frac{De}{Dt} - \frac{P}{\rho^2} \frac{D\rho}{Dt} = \epsilon_{\text{nuc}} - \epsilon_{\nu,\text{nuc}} - \epsilon_{\nu,\text{th}} - \frac{\partial L}{\partial m}. \quad (\text{A19})$$

This is the usual stellar structure equation.

### A.6. MESA Source Terms

Section 3.2 in Paxton et al. (2019) describes the current definition of  $\epsilon_{\text{nuc}}$  in MESA. Importantly, in contrast to the definition given in Equation (A17), MESA already subtracts off the neutrinos in its definition, so the variable `eps_nuc` (provided by the `net` module) is equivalent to  $\epsilon_{\text{nuc}} - \epsilon_{\nu,\text{nuc}}$ . The variable `non_nuc_neu` (provided by the `neu` module) is equivalent to  $\epsilon_{\nu,\text{th}}$ .

The original `weaklib` treatment of weak reactions in MESA (Paxton et al. 2011) included the chemical potential of the electron in  $\epsilon_{\text{nuc}}$ . This term conceptually belongs in  $\epsilon_{\text{grav}}$ , but it was easier to include in  $\epsilon_{\text{nuc}}$  because you can evaluate that contribution as you sum over the reaction rates. One problem with that approach is that it then only includes composition changes due to nuclear reactions. When element diffusion or convective mixing is creating a rate of change in the composition comparable to (or greater than) nuclear reactions and this is occurring in a region where kinetic chemical potentials are important, then MESA will then give the wrong answer. This is a critical shortcoming in the MESA calculations of the simmering phase presented in Martínez-Rodríguez et al. (2016) and is discussed from a different perspective in Schwab et al. (2017).

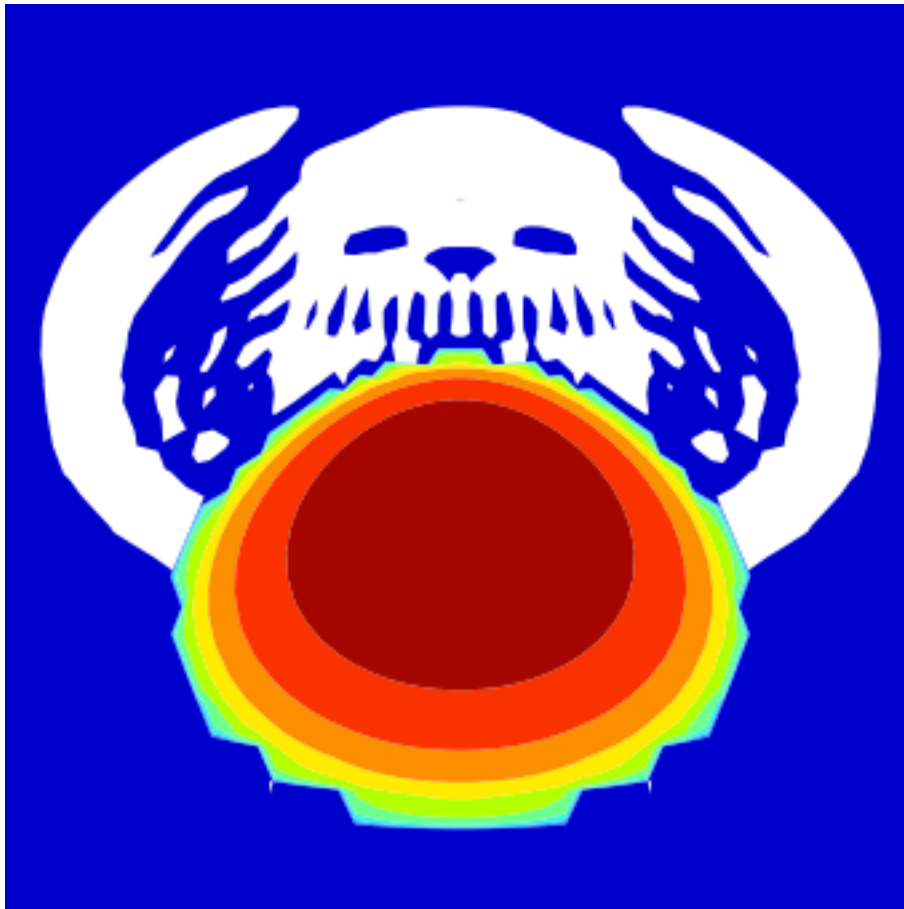
Significant software development effort has gone into correcting this issue and the details are expected to be discussed in a forthcoming MESA instrument paper. In short, the relevant composition-related term can be calculated from a specialized finite difference of the internal energy and included (by default) in  $\epsilon_{\text{grav}}$ . One caveat remains that the thermodynamic basis,  $(\rho, T, \{X_i\})$ , involves the abundances of all isotopes. However, in many cases the EOS basis is not the full composition basis because some component EOSes in MESA reduce the composition basis from all species to a few numbers (e.g.,  $X, Y, Z$  or  $\bar{A}, \bar{Z}$ ). This can limit the ability to calculate the physically relevant energy changes. For example, a change in the metal abundance pattern that left  $Z$  unchanged would be invisible to the EOS. The fact that the new Skye EOS (Jermyn et al. 2021) uses all isotopes with significant mass fractions in its basis means this caveat should not pose a practical concern for future work on this problem using MESA.

## B. AN ASTROPHYSICAL APPARITION: THE PAPALOIZOU-PRINGLE PATRONUS

While in graduate school at Berkeley, I was working on modifying the ZEUS-MP2 code (Hayes et al. 2006) to include an  $\alpha$ -viscosity treatment in preparation for work evolving white dwarf merger remnants (Schwab et al. 2012).

I ran many test problems that followed the evolution of the equilibrium torus solutions considered by Papaloizou & Pringle (1984). During one such experiment, my analysis scripts produced the following contour plot of density. The image has been manipulated only by rotation (such that the equatorial plane is now vertical) and cropping (to focus attention on the relevant feature).

This figure shows the appearance of a powerful and mysterious otter, who is perhaps blowing the fiery bubble that will give rise to our universe. Future work should explore whether spectral methods (e.g., Burns et al. 2020) are more likely to produce such illuminating results.



## REFERENCES

- Badenes, C., Bravo, E., & Hughes, J. P. 2008, *ApJL*, 680, L33, doi: [10.1086/589832](https://doi.org/10.1086/589832)
- Bauer, E. B., Schwab, J., Bildsten, L., & Cheng, S. 2020, *ApJ*, 902, 93, doi: [10.3847/1538-4357/abb5a5](https://doi.org/10.3847/1538-4357/abb5a5)
- Brooks, J., Bildsten, L., Schwab, J., & Paxton, B. 2016, *ApJ*, 821, 28, doi: [10.3847/0004-637X/821/1/28](https://doi.org/10.3847/0004-637X/821/1/28)
- Burns, K. J., Vasil, G. M., Oishi, J. S., Lecoanet, D., & Brown, B. P. 2020, *Physical Review Research*, 2, 023068, doi: [10.1103/PhysRevResearch.2.023068](https://doi.org/10.1103/PhysRevResearch.2.023068)
- Chabrier, G., & Potekhin, A. Y. 1998, *PhRvE*, 58, 4941, doi: [10.1103/PhysRevE.58.4941](https://doi.org/10.1103/PhysRevE.58.4941)
- Chamulak, D. A., Brown, E. F., Timmes, F. X., & Dupczak, K. 2008, *ApJ*, 677, 160, doi: [10.1086/528944](https://doi.org/10.1086/528944)
- Chen, X., Han, Z., & Meng, X. 2014, *MNRAS*, 438, 3358, doi: [10.1093/mnras/stt2439](https://doi.org/10.1093/mnras/stt2439)
- Chugunov, A. I., Dewitt, H. E., & Yakovlev, D. G. 2007, *PhRvD*, 76, 025028, doi: [10.1103/PhysRevD.76.025028](https://doi.org/10.1103/PhysRevD.76.025028)
- Cyburt, R. H., Amthor, A. M., Ferguson, R., et al. 2010, *ApJS*, 189, 240, doi: [10.1088/0067-0049/189/1/240](https://doi.org/10.1088/0067-0049/189/1/240)
- de Groot, S. R., & Mazur, P. 1969, *Non-equilibrium thermodynamics*
- Förster, F., Lesaffre, P., & Podsiadlowski, P. 2010, *ApJS*, 190, 334, doi: [10.1088/0067-0049/190/2/334](https://doi.org/10.1088/0067-0049/190/2/334)
- Gamow, G., & Schoenberg, M. 1940, *Physical Review*, 58, 1117, doi: [10.1103/PhysRev.58.1117](https://doi.org/10.1103/PhysRev.58.1117)
- . 1941, *Physical Review*, 59, 539, doi: [10.1103/PhysRev.59.539](https://doi.org/10.1103/PhysRev.59.539)
- Gasques, L. R., Afanasjev, A. V., Aguilera, E. F., et al. 2005, *PhRvC*, 72, 025806, doi: [10.1103/PhysRevC.72.025806](https://doi.org/10.1103/PhysRevC.72.025806)
- Hayes, J. C., Norman, M. L., Fiedler, R. A., et al. 2006, *ApJS*, 165, 188, doi: [10.1086/504594](https://doi.org/10.1086/504594)
- Hillebrandt, W., & Niemeyer, J. C. 2000, *ARA&A*, 38, 191, doi: [10.1146/annurev.astro.38.1.191](https://doi.org/10.1146/annurev.astro.38.1.191)
- Hix, W. R., & Meyer, B. S. 2006, *Nuclear Physics A*, 777, 188, doi: [10.1016/j.nuclphysa.2004.10.009](https://doi.org/10.1016/j.nuclphysa.2004.10.009)
- Iben, Jr., I. 1978, *ApJ*, 219, 213, doi: [10.1086/155769](https://doi.org/10.1086/155769)
- Jermyn, A. S., Schwab, J., Bauer, E., Timmes, F. X., & Potekhin, A. Y. 2021, *ApJ*, 913, 72, doi: [10.3847/1538-4357/abf48e](https://doi.org/10.3847/1538-4357/abf48e)
- Lesaffre, P., Han, Z., Tout, C. A., Podsiadlowski, P., & Martin, R. G. 2006, *MNRAS*, 368, 187, doi: [10.1111/j.1365-2966.2006.10068.x](https://doi.org/10.1111/j.1365-2966.2006.10068.x)
- Martínez-Rodríguez, H., Piro, A. L., Schwab, J., & Badenes, C. 2016, *ApJ*, 825, 57, doi: [10.3847/0004-637X/825/1/57](https://doi.org/10.3847/0004-637X/825/1/57)
- Martínez-Rodríguez, H., Badenes, C., Yamaguchi, H., et al. 2017, *ApJ*, 843, 35, doi: [10.3847/1538-4357/aa72f8](https://doi.org/10.3847/1538-4357/aa72f8)
- Paczynski, B. 1971, *AcA*, 21, 271
- . 1972, *Astrophys. Lett.*, 11, 53
- . 1973, *AcA*, 23, 1
- Papaloizou, J. C. B., & Pringle, J. E. 1984, *MNRAS*, 208, 721
- Paxton, B., Bildsten, L., Dotter, A., et al. 2011, *ApJS*, 192, 3, doi: [10.1088/0067-0049/192/1/3](https://doi.org/10.1088/0067-0049/192/1/3)
- Paxton, B., Cantiello, M., Arras, P., et al. 2013, *ApJS*, 208, 4, doi: [10.1088/0067-0049/208/1/4](https://doi.org/10.1088/0067-0049/208/1/4)
- Paxton, B., Marchant, P., Schwab, J., et al. 2015, *ApJS*, 220, 15, doi: [10.1088/0067-0049/220/1/15](https://doi.org/10.1088/0067-0049/220/1/15)
- Paxton, B., Schwab, J., Bauer, E. B., et al. 2018, *ApJS*, 234, 34, doi: [10.3847/1538-4365/aaa5a8](https://doi.org/10.3847/1538-4365/aaa5a8)
- Paxton, B., Smolec, R., Schwab, J., et al. 2019, *ApJS*, 243, 10, doi: [10.3847/1538-4365/ab2241](https://doi.org/10.3847/1538-4365/ab2241)
- Piersanti, L., Bravo, E., Cristallo, S., et al. 2017, *ApJL*, 836, L9, doi: [10.3847/2041-8213/aa5c7e](https://doi.org/10.3847/2041-8213/aa5c7e)
- Piro, A. L., & Bildsten, L. 2008, *ApJ*, 673, 1009, doi: [10.1086/524189](https://doi.org/10.1086/524189)
- Piro, A. L., & Chang, P. 2008, *ApJ*, 678, 1158, doi: [10.1086/529368](https://doi.org/10.1086/529368)
- Potekhin, A. Y., & Chabrier, G. 2000, *PhRvE*, 62, 8554, doi: [10.1103/PhysRevE.62.8554](https://doi.org/10.1103/PhysRevE.62.8554)
- Schwab, J., Bildsten, L., & Quataert, E. 2017, *MNRAS*, 472, 3390, doi: [10.1093/mnras/stx2169](https://doi.org/10.1093/mnras/stx2169)
- Schwab, J., Shen, K. J., Quataert, E., Dan, M., & Rosswog, S. 2012, *MNRAS*, 427, 190, doi: [10.1111/j.1365-2966.2012.21993.x](https://doi.org/10.1111/j.1365-2966.2012.21993.x)
- Suzuki, T., Toki, H., & Nomoto, K. 2016, *ApJ*, 817, 163, doi: [10.3847/0004-637X/817/2/163](https://doi.org/10.3847/0004-637X/817/2/163)
- Timmes, F. X., & Swesty, F. D. 2000, *ApJS*, 126, 501, doi: [10.1086/313304](https://doi.org/10.1086/313304)
- Tsuruta, S., & Cameron, A. G. W. 1970, *Ap&SS*, 7, 374, doi: [10.1007/BF00653278](https://doi.org/10.1007/BF00653278)
- Woosley, S. E., Wunsch, S., & Kuhlen, M. 2004, *ApJ*, 607, 921, doi: [10.1086/383530](https://doi.org/10.1086/383530)
- Yakovlev, D. G., Gasques, L. R., Afanasjev, A. V., Beard, M., & Wiescher, M. 2006, *PhRvC*, 74, 035803, doi: [10.1103/PhysRevC.74.035803](https://doi.org/10.1103/PhysRevC.74.035803)